Impact of peatlands on carbon dioxide (CO_2) emissions from the Rajang River and Estuary, Malaysia

Denise Müller-Dum[1], Thorsten Warneke[1], Tim Rixen[2,3], Moritz Müller[4], Antje Baum[2], Aliki Christodoulou[1], Joanne Oakes[5], Bradley D. Eyre[5], and Justus Notholt[1]

[1] Institute of Environmental Physics, University of Bremen, Otto-Hahn-Allee 1, 28359 Bremen, Germany
[2] Leibniz Center for Tropical Marine Research, Fahrenheitstr. 6, 28359 Bremen, Germany
[3] Institute of Geology, University of Hamburg, Bundesstr. 55, 20146 Hamburg, Germany
[4] Swinburne University of Technology, Faculty of Engineering, Computing and Science, Jalan Simpang Tiga, 93350 Kuching, Sarawak, Malaysia
[5] Centre for Coastal Biogeochemistry, School of Environment, Science and Engineering, Southern Cross University, Lismore NSW 2480, Australia

Correspondence to: Denise Müller-Dum, dmueller@iup.physik.uni-bremen.de

Abstract. Tropical peat-draining rivers are known as potentially large sources of carbon dioxide (CO_2) to the atmosphere due to high loads of carbon they receive from surrounding soils. However, not many seasonally resolved data are available, limiting our understanding of these systems. We report the first measurements of carbon dioxide partial pressure (pCO_2) in the Rajang River and Estuary, the longest river in Malaysia. The Rajang River catchment is characterized by extensive peat deposits found in the delta region, and by human impact such as logging, land use and river damming. pCO_2 averaged 2540 ± 189 µatm during the wet season and 2350 ± 301 µatm during the dry season. Using three different parameterizations for the gas transfer velocity, calculated CO_2 fluxes to the atmosphere were 1.5 (0.5-2.0) g C m^{-2} d^{-1} (mean, minimum – maximum) during the wet season and 1.7 (0.6-2.6) g C m^{-2} d^{-1} during the dry season. This is at the low end of reported values for Southeast Asian peat-draining rivers, but similar to values reported for Southeast Asian rivers that do not flow through peat deposits. In the Rajang River, peatlands probably do not contribute much to the CO_2 flux due to the proximity of the peatlands to the coast, which limits the opportunity for degradation of organic C during transport. Thus, we suggest that peat coverage is, by itself, insufficient as sole predictor of CO_2 emissions from peat-draining rivers, and that other factors, like the spatial distribution of peat in the catchment and pH, also need to be considered.

1 Introduction

Tropical rivers transport large amounts of terrestrially derived carbon to the ocean (Dai et al., 2012) and the atmosphere (Aufdenkampe et al., 2011; Raymond et al., 2013). It has been estimated that 78% of riverine carbon dioxide (CO_2) emissions occur in the tropics (Lauerwald et al., 2015). Tropical wetlands exert a particularly strong influence on the carbon budget of these rivers. Two regional studies independently showed that the partial pressure of CO_2 (pCO_2) in rivers increases with increasing wetland coverage in the catchment. Borges et al. (2015) established a relationship between wetland extent and pCO_2 for African rivers. Wit et al. (2015) presented an analog synthesis for Southeast Asian rivers, which flow through peatlands. Peatlands are a special type of wetland, where organic matter accumulates at rates that make them the most effective terrestrial carbon store on a millennial timescale (Dommain et al., 2011). Southeast Asian peatlands store 68.5 Gt carbon (Page et al., 2011). The highest riverine dissolved organic carbon (DOC) concentrations reported so far were found in Southeast Asian peat-draining rivers (Alkhatib et al. 2007; Moore et al., 2011; Müller et al., 2015), with an annual average of 68 mg L^{-1} DOC found in an undisturbed peat-draining river (Moore et al., 2013). Because of these high DOC concentrations, Indonesian rivers may account for 75 % of the DOC flux into the South China Sea (SCS) while accounting for 39 % of the discharge (Huang et al., 2017). Surprisingly, CO_2 emissions from these rivers are not exceptionally high (Müller et al., 2015; Wit et al., 2015). This is attributed to a short residence time of the organic matter in the river, allowing little time for decomposition, and the resistance of peat-derived carbon to bacterial degradation. Nevertheless, the CO_2 flux from peat-draining rivers to the atmosphere increases with increasing peat coverage in the river basin (Wit et al., 2015), showing that these ecosystems exert an important influence on a river's carbon budget.

Most Southeast Asian peat-draining rivers are disturbed by human activities such as river damming, urbanization, deforestation (Milliman and Farnsworth, 2011) and discharge of untreated wastewater (Park et al., 2018). Anthropogenic change poses a new challenge to understanding carbon fluxes in Asian river systems, and more data are urgently needed to constrain the carbon budget for this important region (Park et al., 2018). In Malaysia, the country holding the second largest share of tropical peat (Page et al., 2011), river CO_2 emissions have only been studied in a small undisturbed peat-draining river (Müller et al., 2015), in estuaries (Chen et al., 2013; Müller et al., 2016) and in two river reaches which were not influenced by peat (Müller et al., 2016). In this study, the longest Malaysian river, the Rajang River on the island of Borneo, was investigated. This river flows through largely logged-over tropical rainforest (Gaveau et al., 2014), urban areas and disturbed peat swamps (Gaveau et al., 2016). The aim of this study was to assess the Rajang River and Estuary carbon load and to investigate the impact of peatlands on its CO_2 emissions. To this end, we surveyed longitudinal transects extending from river reaches that were not influenced by peat to the peat-covered delta.

2 Materials and Methods

2.1 Study area

The Rajang River is located in the Malaysian state of Sarawak in the northern part of the island of Borneo (Fig. 1a). Sarawak has a tropical climate with high temperatures (average 26.6°C, 1992-2016 in Sibu, DWD, 2018) and high precipitation (average 3,578 mm yr^{-1}, 1992-2016 in Sibu, DWD, 2018). The region experiences two monsoonal periods: the northeastern monsoon with enhanced rainfall and frequent floods occurs between December and February ("wet season", see Fig. 2a), while the southwestern monsoon from May until September is associated with relatively drier weather ("dry season"). However, despite the monsoon seasons, rainfall is high throughout the year (Sa'adi et al., 2017).

The Rajang River originates in the Iran mountains, a mountain range at the border between Malaysia and Indonesia (MacKinnon, 1996) with elevations of up to 1,800 m (Milliman and Farnsworth, 2011). It drains an area of approximately 52,010 km^2 (Lehner et al., 2006; DID 2017) whose geology is dominated by Cenozoic sedimentary and metamorphic rocks, consisting of siliciclastic rock with minor amounts of carbonates (Staub et al., 2000; Milliman and Farnsworth, 2011). The Rajang River flows approximately 530 km from east to west and discharges into the South China Sea (Milliman and Farnsworth, 2011). Main settlements along the river are the towns of Kapit, Kanowit and the city of Sibu (163,000 inhabitants) (see Fig. 1b). In addition, a large number of longhouses (traditional buildings inhabited by local communities) are located along the river and its tributaries (Ling et al., 2017). Hydroelectric power plants were built on two tributaries in the upper Rajang basin: The Bakun hydroelectric power plant commenced operation in 2011 and the Murum dam in 2015 (Sarawak Energy, 2013, see Fig. 1b). The construction of another hydroelectric power plant on a tributary in the southern Rajang basin is planned for the future (Sarawak Energy, 2013).

The Rajang delta system is comprehensively described in Staub and Gastaldo (2003). It is entirely surrounded by peatlands (Fig. 1b), which extend over an area that corresponds to approximately 11% of the catchment size (Nachtergaele et al., 2009). Most of these peatlands have been converted to industrial oil palm plantations (Gaveau et al., 2016, Fig. 1b). The main distributary channels forming the delta (from north to south) are the Igan, Hulu Seredeng (which splits up into Lassa and Paloh), Belawai and Rajang, which have a maximum tidal range (spring tide) of 3-6 m (Staub and Gastaldo, 2003). Saltwater intrudes into the estuary approximately as far as the point where the Rajang River splits up into its four southernmost distributaries, a few kilometers downstream of Sibu (Fig. 1b), depending on season. Tidal influence extends further inland approximately up to the town of Kanowit (Staub and Gastaldo, 2003).

Monthly discharge (Fig. 2a) was estimated from monthly precipitation (1992-2016; DWD, 2018) and an evapotranspiration rate of 1,545 mm yr^{-1} (Kumagai et al., 2005) or 43.2%. Annual average discharge from 1992-2016 was 3,355 $m^3 s^{-1}$, in good agreement with reported discharges of 3,490 $m^3 s^{-1}$ (Milliman and Farnsworth, 2011) and 3,372 $m^3 s^{-1}$ for the years 1991-2015 (Sa'adi et al, 2017).

2.2 Surveys

We sampled the Rajang River during two surveys, which were designed to get spatial coverage of both peat and non-peat areas during the wettest and driest period of one year. The first survey took place at the peak of the monsoon season in January 2016 ("wet season"). The second one was performed during the dry season in August 2016 ("dry season"). In January 2016, we entered the Rajang River through the Rajang river mouth (distributary 5 in Fig.1b), went upstream to the town of Kapit and back downstream to the town of Belawai at the Belawai river mouth (distributary 4 in Fig. 1b). In August 2016, we entered the Rajang River through the Rajang river mouth (5), went upstream to Kapit and back to Sibu. From there, we went out to the coast through the Lassa distributary (2), and back to Sibu through the Igan distributary (1). The last sampling stretch was from Sibu into the Paloh distributary (3) and back to Belawai (4). During this campaign, one stationary measurement was performed overnight in Sarikei in the Rajang distributary in order to assess tidal/diurnal variability.

2.3 CO_2 measurements

The setup on the boat was similar to the one described in Müller et al. (2016). Surface water was pumped through a shower-type equilibrator (Johnson, 1999) at a rate of approximately 15 L min^{-1}. In the beginning, the equilibrator headspace was connected to an FTIR analyzer (Griffith et al., 2012), which allows for the simultaneous measurement of CO_2, methane (CH_4), nitrous oxide (N_2O) and carbon monoxide (CO). During the cruise in January 2016, a failure of the FTIR analyzer occurred and measurements were continued (also in August 2016) using an Li-820 non-dispersive infrared (NDIR) analyzer for the measurement of CO_2 (Licor, USA). For calibration and inter-calibration of the two instruments, a set of gravimetrically prepared gas mixtures (Deuste Steininger) was measured, which were calibrated against the World Meteorological Organization (WMO) standard scale by the Max Planck Institute for Biogeochemistry in Jena, Germany. For the FTIR, spectra were averaged over 5 minutes and dry air mole fractions were retrieved using the software MALT5 (Griffith 1996). Li-820 data were stored with a temporal resolution of 1 minute. Gas partial pressure was determined using measurements of ambient pressure with a PTB110 barometer (Vaisala, Finland) and correction for removal of water according to Dickson et al. (2007). Water temperature was measured in the equilibrator and in the surface water and correction to water surface temperature was performed according to Dickson et al. (2007).

In August 2016, the internal pressure sensor of the Li-820 failed. Because the instrument performs an internal correction based on the cell pressure, this correction had to be reversed and recalculated with an assumed internal cell pressure. This procedure is described in the Supplement.

CO_2 fluxes (FCO_2, in gC m^{-2} d^{-1}) across the water-air interface were computed using the gas transfer equation

$$FCO_2 = kK_0(pCO_2^{water} - pCO_2^{air}) \cdot f_1 f_2 \quad (1),$$

where k is the gas transfer velocity (m s^{-1}), K_0 is the solubility (mol L^{-1} atm^{-1}) calculated according to Weiss (1974), pCO_2^{water} is the partial pressure of CO_2 in water, pCO_2^{air} is the partial pressure of CO_2 in the overlying air (both in µatm), f_1 is a conversion

factor from L^{-1} to m^{-3}, and f_2 is a conversion factor from µmol s^{-1} to mg d^{-1}. The atmospheric mole fractions of CO_2 during the months of our measurements were derived from the NOAA ESRL Carbon Cycle Cooperative Global Air Sampling Network (Dlugokencky et al., 2018) for the closest station, which was Bukit Kototabang, Indonesia.

The gas transfer velocity (*k*) is a critical, yet poorly constrained parameter. Many studies have attempted to relate *k* to the main drivers of turbulence, such as wind speed (e.g., Wanninkhof, 1992; Nightingale, 2000; Raymond and Cole, 2001) or, especially for rivers, catchment parameters like slope, water flow velocity and discharge (Raymond et al., 2012). We sampled mainly the downstream reaches of the Rajang River, which range in width from 271 m to several kilometers in the delta (Allen and Pavelsky, 2018). Therefore, *k*-parameterizations that were developed for estuaries or big rivers were considered the most appropriate. We compared three parameterizations to constrain the CO_2 fluxes. The first parameterization is the one by Borges et al. (2004) for estuaries, which is driven both by wind speed and water flow velocity; the one by Alin et al. (2011), which was developed for rivers wider than 100 m and is driven by wind speed; and the one by Raymond and Cole (2001), which is driven by wind speed and was developed for big rivers and estuaries. Those parameterizations read:

$$k_{600,B04} = 1.0 + 1.719w^{0.5}h^{-0.5} + 2.58\,u_{10} \quad (2),$$

$$k_{600,A11} = 4.46 + 7.11 \cdot u_{10} \quad (3),$$

$$k_{600,R01} = 1.91 \cdot e^{0.35u_{10}} \quad (4),$$

where *w* is the water flow velocity (cm s^{-1}), *h* is the depth (m) and u_{10} is the wind speed at 10 m (m s^{-1}). *h* was taken from the bottom sounder recordings of our boat. *w* in the lower river reaches was measured by Staub and Esterle (1993) to be 0.7 m s^{-1}. A more recent study by Ling et al. (2017) reports w = 1.1 m s^{-1} for the Rajang River upstream from Kapit. For the calculation of the gas exchange velocity *k*, we used the average of w = 0.9 m s^{-1}. For u_{10}, on-site wind speed data was unfortunately not available. In such cases, other authors (e.g., Bouillon et al., 2012; some estuaries in Chen et al., 2013) have resorted to gridded wind data from the NOAA NCEP NCAR Reanalysis product (Kalnay et al., 1996). While we acknowledge the uncertainty introduced by using gridded data instead of in situ wind speed, we used this product as well, as the best one available for our study area. We retrieved daily wind speed at 10 m for the grid centered at 2.85°N, 112.5°E for the time of our measurements. In-situ *k* is dependent on in-situ salinity and temperature and was calculated from k_{600}, exploiting its relationship with the Schmidt number (Wanninkhof, 1992).

The calculation of fluxes using *k*-parameterizations is associated with a large uncertainty, and it is difficult to determine the most suitable parameterization if none of them was developed in the study region. In addition, using input data from the literature (as for the water flow velocity) or gridded instead of measured wind data adds to this uncertainty (see Supplement). However, using three different parameterizations we are able to constrain the magnitude of CO_2 emissions from the Rajang River. We will report the average CO_2 fluxes from the three different parameterizations as well as minimum and maximum fluxes.

2.4 Ancillary measurements

In January 2016, individual water samples were taken at 15 stations between the river mouth and Kapit, including the distributary channels Rajang and Belawai. In August 2016, water samples were taken at 34 stations, with a higher sampling frequency and coverage in the delta (Rajang, Igan, Lassa, Paloh and Belawai, Fig. 1b). Water samples were taken from approximately 1 m below the surface using a Van Dorn water sampler. Particulate material was sampled on pre-weighed and pre-combusted glass fiber filters. From the net sample weight and the volume of filtered water, the amount of suspended particulate matter (SPM) was determined. For POC, 1N hydrochloric acid was added in order to remove inorganic carbon from the sample. For the determination of carbon, samples were catalytically combusted at 1050°C and combustion products were measured by thermal conductivity using a Euro EA3000 Elemental Analyzer. Repeatability for C content was 0.04 % (standard deviation).

In August 2016, water samples were also taken for the determination of dissolved inorganic carbon (DIC) and the isotopic composition ($\delta^{13}C$) of DIC, because the isotopic composition of DIC can help in identifying its sources (Das et al., 2005; Campeau et al., 2017; 2018). Samples were poisoned with 200 µL concentrated $HgCl_2$ and filtered through Whatman glass fiber filters (GF/F, pore size 0.7 µm). 40 ml sampling vials were filled to the top, leaving no headspace, checked for the existence of bubbles, and stored refrigerated until analysis. Concentrations and $\delta^{13}C$ of DIC were measured via continuous flow wet-oxidation isotope ratio mass spectrometry (CF-WO-IRMS) using an Aurora 1030W TOC analyzer coupled to a Thermo Delta V Plus IRMS (Oakes et al., 2010). Sodium bicarbonate (DIC) of known isotope composition dissolved in helium-purged milli-Q was used for drift correction and to verify concentrations and $\delta^{13}C$ values. Reproducibility for DIC was ±10 µmol L^{-1} for concentrations and ± 0.10‰ for $\delta^{13}C$ (standard deviations).

During both surveys, dissolved oxygen and water temperature were continuously measured with a temporal resolution of 5 minutes using an FDO 925 oxygen sensor and a WTW 3430 data logger (Xylem Inc., USA). The oxygen sensor was calibrated by the manufacturer, a routine function check was performed before the start of measurements using the check and calibration vessel (FDO © Check) provided by the company. The reported accuracy of a dissolved oxygen measurement at 20°C in air-saturated water is 1.5%, the precision of the accompanying temperature measurement is 0.2°C (WTW, 2012). pH, salinity and temperature were measured at the stations, using a SenTix 940 pH sensor (pH) and a Multiprobe (Aquaread AP-2000). The pH sensor was calibrated before the start of the measurements using NIST (National Institute of Standards and Technology) traceable buffers. Since salinity was only measured at the stations, we spatially interpolated salinity for the interpretation of pCO_2 data. This procedure is described in the Supplement.

Different geographical extents of the river were covered during the two campaigns, and the salt intrusion limits were different during the two seasons. In order to keep the results from the two surveys comparable, we report results for three categories: non-peat (Kapit-Kanowit), peat (Kanowit-Sibu) and delta (downstream of Sibu). Their definition and properties are specified in Table 1. The non-peat and peat areas are directly comparable between seasons, because the same spatial extent was covered during both surveys and they were non-saline during both seasons.

2.5 Data analysis and export calculations

Data analysis was performed with Python 2.7.15 and ArcMap 10.5. Averages of measured parameters are reported ± 1 standard error unless stated otherwise. Errors for calculated parameters (e.g., river loads, see below) were determined with error propagation. For fluxes and derived quantities, we report the mean, minimum and maximum from the three *k*-parameterizations. Seasonal differences were tested for significance using the Mann-Whitney U-test from the Python Scipy Statistical Functions module. Data from the delta were excluded from the statistical tests due to the different geographical coverage achieved during the two surveys.

In order to calculate the total carbon export from the Rajang River for the months of our measurements, we derived DOC load, POC load, DIC load for the peat and non-peat area, as well as CO_2 outgassing as follows:

The river loads of DOC, POC and DIC were calculated for the peat and non-peat area combined, using

$$RIVER\ LOAD = C \cdot Q \cdot f_3 \quad (5),$$

where C is the average concentration of DOC/POC/DIC in mg L^{-1}, Q is monthly discharge ($m^3\ s^{-1}$) and f_3 is a conversion factor from s^{-1} to $month^{-1}$.

For DOC, we used the DOC concentrations reported by Martin et al. (2018). This data was acquired during 2017 downstream of Kanowit. Only freshwater values were considered (average for the wet and dry season: 2.0 mg L^{-1} and 2.1 mg L^{-1}). For POC, we used the area-weighted average concentration of peat and non-peat river reaches determined during our surveys.

For DIC, we used an area-weighted average concentration as well, which was determined from our measurements during the dry season. For the wet season survey, DIC was calculated from pH and pCO_2 using the program CO_2sys (Lewis and Wallace, 1998). Note that pH measurements were only available at the stations, and sometimes we did not have parallel pCO_2 measurements. Therefore, the number of calculated DIC values for the peat and non-peat area is 6.

For the calculation of total CO_2 emissions from FCO_2, the river surface area was required. River surface area was calculated from the GRWL (Global River Widths from Landsat) Database (Allen & Pavelsky, 2018) using Esri's ArcMap 10.5. Missing segments in the delta were manually delineated using a Landsat satellite image and their surface area was determined. This procedure is described in the Supplement. With the surface area of individual river segments at hand, CO_2 emissions were calculated for the non-peat area, peat area and the delta separately.

A Keeling plot (Keeling, 1958) was used to explore possible sources of DIC in the Rajang River. The Keeling plot method has been used to determine the isotopic signature in CO_2 from ecosystem respiration (Pataki et al., 2003; van Asperen et al., 2017) by plotting $\delta^{13}C$ of CO_2 in an air sample versus the inverse CO_2 concentration. From the y-intercept of a linear regression, the isotopic signature of the source can be determined (Keeling 1958; Pataki et al., 2003). The Keeling plot method assumes

mixing of only two components: One background component (e.g., atmospheric background) and one additional source (e.g., respiration). While originally designed for atmospheric research, it has also been used in studies exploring possible sources of DIC in stream water (Campeau et al., 2017; 2018). However, it has to be interpreted with caution, because rivers are open systems where the basic assumption of two-component-mixing is easily violated. When we interpret the Keeling plot in this study, we look at mixing between river DIC and added DIC from groundwater and peat-draining rivers. We thus have to assume that DIC in the main river does not change over the time of our measurements. Since the water is continuously replenished from upstream, this assumption is valid as long as the upstream (background) source's isotopic signature remains the same. This can be assumed during a relatively short sampling period (7 days). Nevertheless, we can only consider freshwater data, as mixing with sea water already constitutes a third component. Therefore, we show only freshwater data in our Keeling plot and caution that its interpretation is based on the relatively strong assumption that we can view the river's main stem δ^{13}C-DIC as constant over the sampling period.

3 Results

3.1 General characterization of the Rajang River

Measured salinity ranged between 0 and 18.6 during the wet season and 0 and 32.1 during the dry season. Saltwater was detected further upstream during the dry season than during the wet season (Fig. 3a and b). Saltwater penetrated further inland in the Rajang and Belawai distributaries than in the Igan distributary (Fig. 3b), suggesting that most freshwater is discharged via the Igan distributary.

The Rajang River was slightly acidic (6.7 (wet) and 6.8 (dry), area-weighted mean for the peat and non-peat area, see Table 2) and highly turbid, with area-weighted average SPM concentrations of 187.2 ± 75.7 mg L^{-1} (wet season) and 51.5 ± 12.1 mg L^{-1} (dry season, see Table 2). With higher SPM during the wet season ($p<0.001$), the organic carbon content of SPM was significantly decreased (1.5 ± 0.4 % on average, $p=0.01$) compared to the dry season (2.1 ± 0.6 % on average, see Table 2). POC ranged from 0.7 mg L^{-1} to 9.1 mg L^{-1} during the wet season (average 2.6 ± 0.6 mg L^{-1}) and from 0.3 mg L^{-1} to 1.9 mg L^{-1} during the dry season (average 1.1 ± 0.4 mg L^{-1}, see Table 2). The seasonal difference was significant ($p=0.002$).

The river water was consistently undersaturated with oxygen with respect to the atmosphere. DO oversaturation was not observed. The area-weighted average DO was similar during the wet and dry seasons (81.1 ± 5.5 % and 79.6 ± 3.5 %, wet/dry), with slightly lower DO in the delta (66.0 ± 6.9 % and 71.2 ± 11.1 % (wet/dry)).

Measured DIC in the dry season ranged from 153.7 µmol L^{-1} in the non-peat area to 2399.2 µmol L^{-1} in the estuary and increased linearly with salinity (Fig. 4a, $r = 0.98$, $p<0.001$). Concentrations averaged 177.9 ± 22.4 µmol L^{-1} in the peat and non-peat area and 1302.3 ± 749.2 µmol L^{-1} in the delta (Table 2). Calculated DIC for the wet season averaged 289.8 ± 32.1 µmol L^{-1} (area-weighted mean for the non-peat and peat area). δ^{13}C-DIC ranged between -11.9 ‰ and -1.4 ‰ and averaged –

7.0 ± 1.5 ‰ in the peat and non-peat area and -5.9‰ in the delta (Table 2). δ^{13}C-DIC was positively correlated with DIC for the delta (r = 0.81, p<0.001) and negatively correlated with DIC for the freshwater part (peat and non-peat combined, r = -0.98, p=0.004, Fig. 4b). The Keeling plot for freshwater samples revealed a linear relationship (Fig. 4c) with a y-intercept (± SE) of -18.6 ± 0.3 ‰.

3.2 Carbon dioxide

The Rajang River was oversaturated with CO_2 with respect to the atmosphere, with an average pCO_2 of 2531 ± 188 µatm (wet season) and 2337 ± 304 µatm (dry season) in the non-peat area. pCO_2 was significantly higher in the peat area (p<0.001, both seasons) with 2990 ± 239 µatm (wet season) and 2994 ± 141 µatm (dry season). The area-weighted means for the peat and non-peat area were 2540 ± 189 uatm (wet season) and 2340 ± 301 uatm (dry season). In the delta, pCO_2 was more variable, and the average values of 3005 ± 1039 µatm (wet season) and 2783 ± 1437 µatm (dry season, see Table 2) were also significantly higher than in the non-peat area (p<0.001, both seasons). pCO_2 values were strikingly similar between wet and dry season, and so were the spatial patterns in pCO_2 (Fig. 3c and d). Tidal variability of pCO_2 was observed at an overnight station in Sarikei in August 2016. During this time, pCO_2 increased from approximately 3000 µatm to almost 6000 µatm during rising tide (see Supplement).

pCO_2 decreased with increasing salinity in the delta (Fig.3). However, a big spread of data in both the high-salinity region (during the tidal measurement described above) and the freshwater region was observed. pCO_2 was correlated with DO (Fig. 5). An interesting pattern is consistently visible in both the wet and dry season data, by which main stem data can clearly be distinguished from those collected in the Belawai and Paloh distributaries. Unfortunately, our data did not allow identification of a diurnal signal for either pCO_2 or DO. In the tidal part of the river, we had only one stationary measurement overnight, when a diurnal signal could not be identified due to the strong tidal signal. In the non-tidal part of the river, we had insufficient night-time data to make a statement about a day-night difference for pCO_2 and DO.

Wind speed in the grid centered at 2.85°N, 112.5°E averaged 0.57 m s^{-1} during our campaign in January 2016 and 1.09 m s^{-1} during our campaign in August 2016. The calculated gas exchange velocities for a Schmidt number of 600 using the B04 model ($k_{600, B04}$) were 8.2 cm h^{-1} and 9.6 cm h^{-1}, respectively. This compares to the A11 model with 8.5 cm h^{-1} and 12.2 cm h^{-1} and to the R01 model with 2.3 cm h^{-1} and 2.8 cm h^{-1} for the wet and dry season, respectively. The resultant CO_2 fluxes (FCO_2) to the atmosphere ranged between 0.5 and 2.4 gC m^{-2} d^{-1} in the wet season and between 0.6 and 3.5 gC m^{-2} d^{-1} in the dry season (per water surface unit area, see Table 2).

3.3 Carbon river load and CO_2 emissions

Discharge was above average during 2016 (Fig. 2a). Discharge during January 2016 (wet season) was in accordance with the long-term average, but discharge during August 2016 (dry season) was higher than usual. The Rajang River loads for the peat and non-peat area were 104 (82-123) GgC in January 2016 and 65 (45-83) GgC in August 2016; another 31 (12-41) (wet) and

34 (12-51) Gg were emitted as CO_2 from the delta (Table 3). Of the river loads of carbon, 91 (86-97) % (wet) and 82 (70-94) % (dry) were exported laterally by discharge. Approximately half of the laterally transported carbon was in the organic form (57 ± 12% and 60 ± 18%, wet/dry). River loads were similar during both seasons, except that POC export was 3-fold higher in the wet season. CO_2 emissions to the atmosphere accounted for 9 (3-14) % and 18 (6-30) % (wet/dry) of the total carbon load of the river.

4. Discussion

4.1 Sediment yield and organic carbon load

The Asia-Pacific region is known for its high sediment yields, especially where rivers drain Cenozoic sedimentary and volcanic rock (Milliman and Farnsworth, 2011). Therefore, the high suspended sediment load in the Rajang River is not surprising. However, SPM concentrations during our expeditions were substantially lower (187.2 ± 75.7 mg L^{-1} and 51.5 ± 12.1 mg L^{-1}) than in July 1992 (613 mg L^{-1}, Staub and Esterle, 1993). This could be an effect of upstream dams (operational since 2011 and 2015), which trap sediment in their reservoirs, thereby reducing downstream sediment loads (Vörösmarty et al., 2003, Snoussi et al., 2002). In support of this, SPM concentrations were intermediate in the upper Rajang River in 2014/2015 (218.3 mg L^{-1}; Ling et al., 2017). These measurements were taken before, and the measurements in the current study were taken after, the Murum dam began full operation in the second quarter of 2015. Furthermore, SPM and POC concentrations (2.6 mg L^{-1} and 1.1 mg L^{-1}, wet/dry) in the Rajang River were similar to those in the Pearl River, China, (SPM: 70 mg L^{-1} -247 mg L^{-1}, POC: 1.0 mg L^{-1} -3.8 mg L^{-1}, Ni et al., 2008) and the Red River, Vietnam, (SPM: 294 ± 569 mg L^{-1} (wet) and 113 ± 428 mg L^{-1} (dry), POC: 3.7 ± 2.0 mg L^{-1} (wet) and 1.1 ± 1.1 mg L^{-1} (dry), Le et al., 2017), both of which are also affected by damming.

SPM was higher during the wet season than during the dry season in agreement with observations at the Kinabatangan River, Malaysia (Harun et al., 2014). This can be attributed to enhanced erosion during the wet season. In logged-over forest, as found in most of the Rajang River basin, the energy impact of rain drops on the soil is higher than in densely vegetated areas, where rain is intercepted by the canopy before falling on the ground (Ling Lee et al., 2004). In agreement with this line of reasoning, Ling et al. (2016) showed that the amount of suspended solids in Malaysian streams draining areas with logging activities increased significantly after rain events. The decreased organic carbon content observed during the wet season further supports this, as it indicates a higher contribution of eroded mineral soil to SPM. This pattern is observed in many rivers in this region (Huang et al., 2017). Despite the changing carbon content, most POC was still exported during the wet season, as in other Southeast Asian rivers (Ni et al., 2008; Moore et al., 2011). The proportion of laterally transported carbon in the Rajang River that is in organic form (57 ± 12 % and 60 ± 18%, wet/dry) is similar to that reported for the carbon flux to the South China Sea (50 ± 14%, Huang et al., 2017).

4.2 Inorganic carbon load

4.2.1 DIC concentrations and sources

DIC concentrations measured during our dry season survey were comparable to those determined by Huang et al. (2017) for the Rajang River (201 µmol L^{-1} and 487 µmol L^{-1}). Their values are based on 7 measurements taken between 2005 and 2009 downstream of Sibu (pers. comm.). DIC concentrations in the Rajang River thus appear to be substantially lower than in the Mekong River (1173-2027 µmol L^{-1}, Li et al., 2013) and the Pearl River (1740 µmol L^{-1}, Huang et al., 2017), but similar to those in the Musi River, Indonesia (250 µmol L^{-1}, Huang et al., 2017). This suggests that the Rajang River compares better to the equatorial Indonesian rivers than to rivers draining mainland Southeast Asia, probably because of the scarcity of carbonate rock, which has the highest weathering rate and is thus responsible for high DIC in rivers (Huang et al., 2012).

The source of DIC varied along the length of the Rajang River. In the estuarine part, the positive linear relationship between DIC and salinity (Fig. 4a) suggests that the main source of DIC in the estuary is marine. This is also supported by the relatively high δ^{13}C-DIC of estuarine samples, as ocean DIC is more enriched, with δ^{13}C-DIC between 0 and 2.5 ‰ (Rózanski et al., 2003). The positive correlation between DIC and δ^{13}C in the delta thus implies an increasing contribution of marine DIC.
In the freshwater part of the Rajang River, δ^{13}C values were more depleted (-7.0 ± 1.5 ‰, Table 2) than downstream, but were more enriched than δ^{13}C-DIC values reported for other rivers in the region (Lupar and Saribas Rivers in Sarawak, -15.7 ‰ to -11.4 ‰, Müller et al., 2016; Musi, Indragiri and Siak Rivers in Indonesia, -22.5 ‰ to -9.0 ‰, Wit, 2017).

Multiple sources and processes are likely to influence δ^{13}C-DIC in the Rajang River. To start with, the y-intercept of the Keeling plot for freshwater samples suggests that the DIC added to the main river has a δ^{13}C of -18.6 ‰, which is consistent with δ^{13}C values of bicarbonate from silicate weathering with soil CO_2 from C3 plants (-22.1 to -16.1 ‰, Das et al., 2005), i.e. groundwater input.

Another relevant source is rainwater DIC with a typical δ^{13}C of -9.3 ‰ (Das et al., 2005). In a river with relatively low DIC (177.9 µmol L^{-1}) and large surface runoff due to heavy rain, this source term is presumably non-negligible, and a significant contribution would partially explain the relatively high δ^{13}C-DIC values.

With regard to in-stream processes, photosynthesis increases and respiration decreases δ^{13}C-DIC (Campeau et al., 2017). Due to the high turbidity, it can be assumed that photosynthesis in the Rajang River is negligible. In contrast, the correlation of DO and pCO_2 (Fig. 5) suggests that respiration is important. This assumption is supported by the negative correlation of δ^{13}C and DIC for freshwater samples, because with increasing DIC, δ^{13}C values get more depleted, suggesting that organic carbon (with a δ^{13}C of around -26 ‰ for C3 plants, Rózanski et al., 2003) is respired to CO_2 within the river. However, we observed overall relatively high δ^{13}C values. Two processes are likely to be responsible for the downstream increase in δ^{13}C: (1) Methanogenesis and (2) evasion of CO_2. (1) Campeau et al. (2018) observed a strong relationship between CH_4 concentration and δ^{13}C-DIC in a boreal stream draining a nutrient-poor fen, suggesting that fractionation during methanogenesis leads to an increase in δ^{13}C-DIC. As the peat soils in the Rajang delta are also anaerobic and nutrient-poor, it is likely that methanogenesis plays a role

there as well. This is consistent with high reported soil CH_4 concentrations of up to 1465 ppm in a peat under an oil palm plantation in Sarawak (Melling et al., 2005). It would therefore be of high interest to investigate CH_4 concentrations in the Rajang River in the future. (2) CO_2 evasion is also known to lead to a gradual increase of δ^{13}C-DIC values until in equilibrium with the atmosphere (with a slightly positive δ^{13}C-DIC, Polsenare and Abril, 2012; Venkiteswaran et al., 2014; Campeau et al., 2018). Due to intracarbonate equilibrium fractionation, dissolved CO_2 is more depleted in δ^{13}C than the other carbonate species. Thus, if it is removed, δ^{13}C of the remaining DIC increases. This effect depends on pH and is more pronounced in near-neutral waters and less strong in very acidic water (Campeau et al., 2018). We sampled the lower river reaches downstream of Kapit, which corresponds to approximately the last 200 kilometers of the river. In addition, the terrain is much steeper upstream of Kapit than in the lower river reaches, so that CO_2 fluxes to the atmosphere are presumably much higher due to higher turbulence. This means that a large fraction of CO_2 had likely already been emitted from the river surface before reaching Kapit, leading to the observed high δ^{13}C-DIC values.

4.2.2 pCO_2

pCO_2 in the Rajang River was higher than in most Southeast Asian rivers without peat influence, such as the Mekong River (pCO_2= 1090 µatm, Li et al., 2013), the Red River (pCO_2= 1589 µatm, Le et al., 2017) or the freshwater parts of the Lupar and Saribas Rivers (pCO_2= 1274 µatm and 1159 µatm, Müller et al., 2016, Table 4, Fig. 6). This could be attributed to the peat influence. However, the Rajang River has a pCO_2 at the low end of values reported for peat-draining rivers (Fig. 6): Wit et al. (2015) report values between 2400 µatm in the Batang Hari (peat coverage = 5%) and 8555 µatm in the Siak River (peat coverage = 22%).

A meaningful comparison is also the one between the Rajang River and the Indragiri River, Indonesia, because they have a similar peat coverage (Rajang: 11%, Indragiri: 12%) and peat coverage has previously been considered as a good predictor of river CO_2 emissions (Wit et al., 2015). However, pCO_2 in the Indragiri (5777 µatm) was significantly higher than in the Rajang, which was associated with a lower pH (6.3, numbers from Wit et al., 2015). A simple exercise using CO_2Sys illustrates how important it is to consider both pH and pCO_2 when comparing different peat-draining rivers. At the given temperature, salinity and pH, the pCO_2 of 5777 µatm in the Indragiri corresponds to a DIC value of 327 µmol L^{-1}. At a hypothetical pH of 6.8, as measured in the Rajang River, this DIC value corresponds, under otherwise unchanged conditions, to a pCO_2 of 2814 µatm – which is very close to the average values measured in the peat area of the Rajang River. The close coupling of pH and pCO_2 implies that peat coverage in a river basin is insufficient as sole predictor of CO_2 fluxes. Rather, the relationship between peat coverage and pCO_2 must be viewed in the context of the rivers' pH, and drivers of pH must be more carefully considered. Note also that peat coverage is usually reported for the entire catchment (e.g., Wit et al, 2015; Rixen et al., 2016) and does not reveal how much peat is found in estuarine vs. freshwater reaches, which complicates comparisons further.

δ^{13}C-DIC in the Indragiri was lower (-16.8 ‰, Wit, 2017) than in the Rajang (-7.0 ‰). While this can be partially attributed to the different pH, it can also be interpreted as a greater contribution of respiratory CO_2 in the Indragiri, while the Rajang might be more strongly influenced by weathering. This would also help to explain the higher pH in the Rajang River.

While DOC and pCO_2 are positively related to discharge in most rivers (e.g., Bouillon et al., 2012), this pattern is sometimes reversed in peat-draining rivers. This is due to dilution, when rainfall exceeds the infiltration capacity of the wet soil and water runs off at the surface (Clark et al., 2008; Rixen et al., 2016). In the Rajang River, pCO_2 was slightly higher in the non-peat area during the wet season in agreement with many non-peat-draining tropical rivers (Bouillon et al., 2012; Teodoru et al., 2014; Scofield et al., 2016). However, the seasonality of pCO_2 was very small, similar to other Malaysian rivers (Müller et al., 2016) and in line with the small seasonal variability of DOC concentrations in the Rajang River (Martin et al., 2018). Note that since our data was collected during two single surveys, they represent only a snapshot and do not allow strong claims about seasonality.

Due to an El Nino event, temperatures in Southeast Asia were unusually high in late 2015 and 2016, with a temperature extreme in April 2016 prevailing in most of Southeast Asia (Thirumalai et al., 2017) and unusually hot conditions also recorded in Sibu (Fig. 2b). Given that weathering rates increase at elevated temperatures, DIC from weathering could have been enhanced over other years, although this seems unlikely because DIC was relatively low and in agreement with previous studies. Another factor to be taken into account is that decomposition in the dry upper soil layer is more intense at higher temperatures, and with incipient rainfall, all the resultant DOC is flushed out to the river. Therefore, it is possible that during the year of our measurements, DOC concentrations were higher than usual, and respiratory CO_2 may therefore have been enhanced compared to other years.

4.2.3 Impact of the peatlands on the CO_2 emissions from the Rajang River

The fact that pCO_2 was significantly higher in the peat area than in the non-peat area implies, at first glance, that the peat areas are a source of CO_2 to the river. However, this difference has to be interpreted with caution, as the entire peat area is under tidal influence (Fig. 1b). In the following, we will present several arguments that suggest that the peatlands exert only a small influence on the CO_2 emissions from the Rajang River.

a) DOC

One indicator of peatland influence on a river's carbon budget is DOC. DOC concentrations in the Rajang River delta were reported to range between 1.4 mg L^{-1} and 3 mg L^{-1} (Martin et al., 2018). This is at the low end of the range of DOC concentrations reported for peat-draining rivers in Indonesia: These range from 2.9 mg L^{-1} in the Musi River (peat coverage = 3.5%) up to 21.9 mg L^{-1} in the Siak River (peat coverage = 22%; Wit et al., 2015). Rivers whose catchment area is entirely covered by peat exhibit even higher DOC concentrations, with 52 mg L^{-1} (wet season) and 44 mg L^{-1} (dry season) in the Sebangau River, Indonesia (Moore et al., 2011), and 44 mg L^{-1} in the Maludam River, Sarawak, Malaysia (Müller et al., 2015).

The Rajang River compares rather to rivers like Lupar and Saribas, Malaysia, which exhibit DOC concentrations of 1.8 mg L^{-1} and 3.7 mg L^{-1} in their freshwater parts (no peat influence, Müller et al., 2016). Consequently, DOC concentrations imply that the peatlands' influence on the Rajang's DOC is rather small.

b) Mixing model

An alternative approach is to theoretically calculate the increase in Rajang River pCO_2 that would result from the influx from peatlands. For this, we created a simple model to simulate the mixing of two water masses (see Supplement), one with a pH of 6.8 and a pCO_2 of 2434 µatm (designed to resemble the Rajang River, non-peat area) and the other with a pH of 3.8 and a pCO_2 of 8100 µatm (designed to resemble peat-draining tributaries, based on values for the peat-draining Maludam River in Sarawak, Müller et al., 2015). For simplicity, we assumed that mixing occurs at salinity = 0 and that the temperature in both water bodies is the same (28.4°C). From these values, DIC and total alkalinity (TA) of the two water bodies were calculated using CO_2Sys. Since they can be assumed to be conservative, we simply calculated DIC and TA of the mixture as

$$DIC_{S=0} = (1 - pc) \cdot DIC_1 + pc \cdot DIC_2 \text{ and } TA_{S=0} = (1 - pc) \cdot TA_1 + pc \cdot TA_2 \quad \text{(8) and (9),}$$

where *pc* is the peat coverage in the basin (*pc*=0.11). From DIC and TA, the pCO_2 of the mixture was computed (pCO_2 = 3058 µatm). This means that if all peat-draining tributaries in the Rajang River basin had a pCO_2 of 8100 µatm and a pH of 3.8, the pCO_2 in the peat area would be enhanced by around 600 µatm. However, this increase in pCO_2 is obviously gradual. For example, at the city of Sibu, peat coverage was estimated at around 2%, for which the described mixing model yields a pCO_2 of 2548 µatm (Fig. S3). In most parts of the delta, dilution with sea water already plays a role. Therefore, the mixing model was extended, assuming that at *pc*=3%, salinity is still zero and then linearly increases until *pc*=11%, *S* = 32, $DIC_{S=32}$ = 2347 µmol L^{-1} and $TA_{S=32}$ = 2324 µmol L^{-1} (two end-member mixing model, see Supplement). As a result, pCO_2 would theoretically not exceed 2605 µatm if the peat-draining tributaries were the only source of CO_2 downstream of Kanowit (Fig. S3).

However, pCO_2 in the peat area was 2990 µatm (wet) and 2994 µatm (dry) and 3005 µatm (wet) and 2783 µatm (dry) in the delta, so there must be another source of CO_2. Since pCO_2 in Sarikei varied 2-fold with the tidal cycle, it seems likely that a large part of the difference in pCO_2 between non-peat area and peat area is actually a difference between river and tidal river. Tidal variability is often seen in estuaries (e.g., Bouillon et al., 2007, Oliveira et al., 2017), largely due to conservative mixing. However, during rising tide in Sarikei, we observed pCO_2 values of almost 6000 µatm, which is higher than the freshwater end-member, suggesting that other effects also play a role. Among those are decomposition of organic matter in intertidal sediments (Alongi et al., 1999, Cai et al., 1999) and subsequent transport of the produced CO_2 to the river, as well as groundwater input (Rosentreter et al., 2018).

c) δ^{13}C-DIC

If the peatlands acted as a significant source of CO_2 to the Rajang River, it would be expected that this had an impact on the δ^{13}C-DIC values. In the peat-draining Maludam River, δ^{13}C-DIC averaged -28.55 ‰ (Müller et al., 2015). Thus, the influx of peat-draining tributaries to the Rajang River (with an average δ^{13}C-DIC of -7‰) would theoretically decrease δ^{13}C-DIC. This was not observed. Instead, the main source identified by the Keeling plot was consistent with groundwater input with a δ^{13}C-DIC of -18.6 ‰. However, given the constraints on the applicability of the Keeling plot method discussed above, the effect of DIC inputs from peat on the δ^{13}C-DIC might simply not be detectable. Other processes which influence δ^{13}C-DIC as discussed above might also prevent identification of a peat signal in the δ^{13}C-DIC data.

In summary, we were unable to discern a large impact of peatlands on the DIC budget of the Rajang River. It is possible that, because the peatlands are located close to the coast in this system, mixing with sea water occurs before significant effects on the pCO_2 are theoretically possible. This means that not only the peat coverage in the catchment is relevant, but also how much of this peat is found in estuarine reaches. These findings support the arguments of Müller et al. (2015) and Wit et al. (2015) that material derived from coastal peatlands is swiftly transported to the ocean, explaining why peat-draining rivers may not necessarily be strong sources of CO_2 to the atmosphere.

5. Conclusions

The Rajang River is a typical Southeast Asian river, transporting large amounts of terrestrial material to the South China Sea. In contrast to other Southeast Asian rivers with similar peat coverage, the impact of the peatlands on the Rajang River's pCO_2 appeared to be rather small, probably due to the proximity of the peatlands to the coast. As a consequence, CO_2 emissions from the Rajang River were moderate compared to other Southeast Asian rivers and low if compared to Southeast Asian peat-draining rivers.

Data availability

Calibrated data used in this manuscript are available as a Supplementary Table to this manuscript. Raw data are available at the Institute of Environmental Physics, University of Bremen, Bremen, Germany.

Author contribution

DMD, TW, TR and MM designed this study. DMD performed all measurements and sample preparations during the first survey, AC, AB and MM performed the measurements and sample preparations during the second survey. JO and BE analyzed the DIC and isotopic data, DMD analyzed all other data. All co-authors contributed to the interpretation and discussion of the results. DMD prepared the manuscript with contributions from all co-authors.

Competing interests

The authors declare that they have no conflict of interest.

Acknowledgements

We would like to thank the Sarawak Biodiversity Centre for permission to conduct research in Sarawak waters (permit no. SBC-RA-0097-MM and export permits SBC-EP-0040-MM and SBC-EP-0043-MM). We also thank Dr. Aazani Mujahid (University of Malaysia Sarawak, Kuching, Malaysia) for her extensive organizational help in preparing the campaigns. Further, we would like to thank all students and scientists from Swinburne University of Technology and UNIMAS in Malaysia for their help during the sampling trips. Lukas Chin and the "SeaWonder" crew are acknowledged for their support during the cruises. The study was supported by the Central Research Development Fund of the University of Bremen, the MOHE FRGS Grant (FRGS/1/2015/WAB08/SWIN/02/1), SKLEC Open Research Fund (SKLEC-KF201610) and ARC Linkage Grant LP150100519.

References

Alin, S. R., de Fátima F. L. Rasera, M., Salimon, C., I., Richey, J. E., Holtgrieve, G. W., Krusche A. V., and Snidvongs, A. Physical controls on carbon dioxide transfer velocity and flux in low-gradient river systems and implications for regional carbon budgets. J Geophys Res 116, G01009, doi: 10.1029/2010JG001398, 2011.

Alkhatib, M., Jennerjahn, T. C., and Samiaji, J. Biogeochemistry of the Dumai River Estuary, Sumatra, Indonesia, a Tropical Black-Water River. Limnol Oceanogr 52(6): 2410-2417, 2007.

Allen, G. H. and Pavelsky, T. M. Global extent of rivers and streams. Science 361, 585-588, doi: 10.1126/science.aat0636, 2018.

Alongi, D. M., Tirendi, F., Dixon, P., Trott, L. A., and Brunskill, G. J. Mineralization of Organic Matter in Intertidal Sediments of a Tropical Semi-enclosed Delta. Estuar Coast Shelf S 48: 451-467, 1999.

Aufdenkampe, A. K., Mayorga, E., Raymond, P. A., Melack, J. M., Doney, S. C., Alin, S. R., Aalto, R. E., and Yoo, K. Riverine coupling of biogeochemical cycles between land, oceans, and atmosphere. Front Ecol Environ 9(1): 53-60. doi: 10.1890/100014, 2011.

Borges, A. V., Vanderborght, J.-P., Schiettecatte, L.-S., Gazeau, F., Ferrón-Smith, S., Delille, B., and Frankignoulle, M. Variability of the Gas Transfer Velocity of CO_2 in a Macrotidal Estuary (the Scheldt). Estuaries 27(4): 593-603, 2004.

Borges, A. V., Abril, G., Darchambeau, F., Teodoru, C. R., Deborde, J., Vidal, L. O., Lambert, T., and Bouillon, S. Divergent biophysical controls of aquatic CO_2 and CH_4 in the World's two largest rivers. Nature Sci Rep 5:15614. doi: 10.1038/srep15614, 2015.

Bouillon, S. Middelburg, J. J., Dehairs, F., Borges, A. V., Abril, G., Flindt, M. R., Ulomi, S. and Kristensen, E., Importance of intertidal sediment processes and porewater exchange on the water column biogeochemistry in a pristing mangrove creek (Ras Dege, Tanzania). Biogeosciences 4: 311-322, 2007.

Bouillon, S., Yambélé, A., Spencer, R. G. M., Gilikin, D. P., Hernes, P J., Six, J., Merckx, R., and Borges, A. V. Organic matter sources, fluxes and greenhouse gas exchange in the Oubangui River (Congo River basin). Biogeosciences 9, 2045-2062. doi: 10.5194/bg-9-2045-2012, 2012.

Cai, W.-J., Pomeroy, L.R., Moran, M. A., and Wang, Y. Oxygen and carbon dioxide mass balance for the esuarine-intertidal marsh complex of five rivers in the southeastern U.S. Limnol Oceanogr 44(3): 639-649, 1999.

Campeau, A., Wallin, M. B., Giesler, R., löfgren, S., Mörth, C.-M., Schiff, S., Venkiteswaran, J. J., and Bishop, K. Multiple sources and sinks of dissolved inorganic carbon across Swedish streams, refocusing the lens of stable C isotopes. Nature Sci Rep 7:9158. doi: 10.1038/s41598-017-09049-9, 2017.

Campeau, A., Bishop, K., Nilsson, M. B., Klemedtsson, L., Laudon, H., Leith, F. I., Öquist, M., and Wallin, M. B. Stable carbon iosotopes reveal soil-stream DIC linkages in contrasting headwater catchments. J Geophys Res-Biogeo 123: 149-167, doi: 10.1002/2017JG004083, 2018.

Chen, C.-T. A., Huang, T.-H., Chen, Y.-C., Bai, Y., He, X. and Kang, Y. Air-sea exchanges of CO_2 in the world's coastal seas. Biogeosciences 10: 6509-6544. doi: 10.5194/bg-10-6509-2013, 2013.

Clark, J. M., Lane, S. N., Chapman, P. J., and Adamson, J. K. Link between DOC in near surface peat and stream water in an upland catchment. Sci Total Environ 404(2-3): 308-315. doi: 0.1016/j.scitotenv.2007.11.002, 2008.

Dai, M., Yin, Z., Meng, F., Liu, Q., and Cai, W.-J. Spatial distribution of riverine DOC inputs to the ocean: an updated global synthesis. Curr Opin Env Sust 4: 170-178. doi: 10.1016/j.cosust.2012.03.003, 2012.

Das, A., Krishnaswami, S., and Bhattacharya, S. K. Carbon isotope ratio of dissolved inorganic carbon (DIC) in rivers draining the Deccan Traps, India: Sources of DIC and their magnitudes. Earth Planet Sc Lett 236: 419-429, 2005.

Dickson, A., Sabine, C., and Christian, G. Guide to best practices for ocean CO_2 measurements. North Pacific Marine Science Organization (PICES) Special Publication, 191 pp., 3rd edition. http://cdiac.ess-dive.lbl.gov/ftp/oceans/Handbook_2007/Guide_all_in_one.pdf (last access: 29th June 2018), 2007.

DID: Department of Irrigation and Drainage Sarawak: Resource Centre-IRBM 22 Basins. http://www.did.sarawak.gov.my/modules/web/pages.php?mod=webpage&sub=page&id=315&menu_id=0&sub_id=314 (last access: 29th June 2018), 2017.

Dlugokencky, E. J., Lang, P. M., Mund, J. W., Crotwell, A. M., Crotwell, M. J., and Thoning, K. W. Atmospheric carbon dioxide dry air mole fractions from the NOAA ESRL Carbon Cycle Cooperative Global Air Sampling Network, 1968-2016, Version: 2017-07-28, Path: ftp://aftp.cmdl.noaa.gov/data/trace_gases/co2/flask/surface/ (last access: 06/13/2018), 2018.

Dommain, R., Couwenberg, J., and Joosten, H. Development and carbon sequestration of tropical peat domes in south-east Asia: links to post-glacial sea-level changes and Holocene climate variability. Quaternary Sci Rev 30: 999-1010. doi: 10.1016/j.quascirev.2011.01.018, 2011.

DWD: German Weather Service: Climate data center, path: ftp://ftp-cdc.dwd.de/pub/CDC/observations_global/CLIMAT/ (last access: 27th Aug, 2018), Station ID 96421, 2018.

Gaveau, D. L. A., Sloan, S., Molidena, E., Yaen, H., Sheil, D., Abram, N. K., Ancrenaz, M., Nasi, R., Quinones, M., Wielaard, N., and Meijaard, E. Four Decades of Forest Persistence, Clearance and Logging on Borneo. PlosOne 9(7): e101654. doi: 10.1371/journal.pone.0101654, 2014.

Gaveau, D.L.A.; Salim, M.; Arjasakusuma, S.: Deforestation and industrial plantations development in Borneo, Center for International Forestry Research (CIFOR), V2; REGBorneo_PlantedIOPP_1973to2016_CIFOR, doi: 10.17528/CIFOR/DATA.00049, 2016.

Griffith, D. W. T. Synthetic calibration and quantitative analysis of gas-phase FT-IR spectra. Applied Spectroscopy 50: 59-70, 1996.

Griffith, D. W. T., Deutscher, N. M., Caldow, C., Kettlewell, G., Riggenbach, M., and Hammer, S. A Fourier transform infrared trace gas and isotope analyser for atmospheric applications. Atmos Meas Tech, 5:2481–2498. doi: 10.5194/amt-5-2481-2012, 2012.

Harun, S., Dambul, R., Abdullah, M. H., and Mohamed, M. Spatial and seasonal variations in surface water quality of the Lower Kinabatangan River Catchment, Sabah, Malaysia. Journal of Tropical Biology and Conservation 11: 117-131. ISSN 1823-3902, 2014.

Huang, T. H., Fu, Y. H., Pan, P. Y., and Chen, C. T. A. Fluvial carbon fluxes in tropical rivers. Curr Opin Env Sust 4: 162-169, doi: 10.1016/j.cosust.2012.02.004, 2012.

Huang, T. H., Chen, C. T. A, Tseng, H. C., Lou, J. Y., Wang, S. L., Yang, L., Kandasamy, S., Gao, X., Wang, J. T., Aldrian, E., Jacinto, G. S., Anshari, G. Z., Sompongchaiyakul, P., and Wang, B. J. Riverine carbon fluxes to the South China Sea. Journal of Geophysical Research: Biogeosciences 122: 1239-1259. doi: 10.1002/2016JG003701, 2017.

Johnson, J. E. Evaluation of a seawater equilibrator for shipboard analysis of dissolved oceanic trace gases. Anal Chim Acta 395: 119-132, 1999.

Kalnay, E., Kanamitsu, M., Kistler, R., Collins, W., Deaven, D., Gandin, L., Iredell, M., Saha, S., White, G., Woollen, J., Zhu, Y., Chelliah, M., Ebisuzaki, W., Higgins, W., Janowiak, J., Mo, K. C., Ropelewski, C., Wang, J., Leetmaa, A., Reynolds, R. Jenne, R., and Joseph, D. The NCEP/NCAR 40-year reanalysis project, Bull. Amer. Meteor. Soc., 77, 437-470, 1996.

Keeling, C. D. The concentration and isotopic abundances of atmospheric carbon dioxide in rural areas. Geochimica et Cosmoschimica Acta, 13: 322-334, 1958.

Kumagai, T., Saitoh, T. M., Sato, Y., Takahashi, H., Manfroi, O. J., Morooka, T., Kuraji, K., Suzuki, M., Yasunari, T., and Komatsu, H. Annual water balance and seasonality of evapotranspiration in a Bornean tropical rainforest. Agr Forest Meteorol, 128: 81–92. doi: 10.1016/j.agrformet.2004.08.006, 2005.

Lauerwald, R., Laruelle, G. G., Hartmann, J., Ciais, P., and Regnier, P. A. G. Spatial patterns in CO_2 evasion from the global river network. Global Biogeochem Cy, 29:1–21. doi: 10.1002/2014GB004941, 2015.

Le, T. P. Q., Dao, V. N., Rochelle-Newall, E., Garnier, J., Lu, X., Billen, G., Duong, T. T., Ho, C. T., Etcheber, H., Nguyen, T. M. H., Nguyen, T. B. N., Nguyen, B. T., Le, N. D., and Pham, Q. L. Total organic carbon fluxes of the Red River System (Vietnam). Earth Surf Proc Land 42: 1329-1341. doi: 10.1002/esp.4107, 2017.

Le, T. P. Q., Marchand, C., Ho, C. T., Duong, T. T., Nguyen, H. T. M., XiXi, L. Vu, D. A., Doan, P. K., and Le, N. D. CO_2 partial pressure and CO_2 emissions along the lower Red River (Vietnam). Biogeosciences 15: 4799-4814, doi: 10.5194/bg-15-4799-2018, 2018.

Lehner, B, Verdin, K., and Jarvis, A. HydroSHEDS technical documentation. World Wildlife Funds US, Washington, D. C., 1 edition. http://hydrosheds.cr.usgs.gov (last access: 29th June 2018), 2006.

Lewis, E., and D. W. R. Wallace. Program Developed for CO_2 System Calculations. ORNL/CDIAC-105. Carbon Dioxide Information Analysis Center, Oak Ridge National Laboratory, U.S. Department of Energy, Oak Ridge, Tennessee, 1998.

Li, S., Lu, X. X., and Bush, R. T. CO_2 partial pressure and CO_2 emission in the Lower Mekong River. J Hydrol 504: 40-56. doi: 10.1016/j.jhydrol.2013.09.024, 2013.

Ling, T.-Y., Soo, C.-L., Sivalingam, J.-R., Nyanti, L., Sim, S.-F., and Grinang, J. Assessment of the water and sediment quality of tropical forest streams in upper reaches of the Baleh River, Sarawak, Malaysia, subjected to logging activities. J Chem-NY, Article ID 8503931. doi: 10.1155/2016/8503931, 2016.

Ling, T.-Y., Soo, C.-L., Phan, T.-P., Nyanti, L., Sim, S.-F., and Grinang, J. Assessment of Water Quality of Batang Rajang at Pelagus Area, Sarawak, Malaysia. Sains Malays 46(3): 401-411. doi: 10.17576/jsm-2017-4603-07, 2017.

Ling Lee, H., Koh, H. L. and Al'Rabia'ah, H. A. Predicting soil loss from logging in Malaysia. GIS and Remote Sensing in Hydrology, Water Resources and Environment. Proceedings of ICGRHWE held at the Three Gorges Dam, China, September 2003. IAHS Publ. 289, 2004.

MacKinnon, K.: The ecology of Kalimantan. In: The ecology of Indonesia series, Vol. 3. Oxford University Press, Oxford 1996.

Martin, P., Cherukuru, N., Tan, A. S. Y., Sanwlani, N., Mujahid, A., and Müller, M. Distribution and cycling of terrigenous dissolved organic carbon in peatland-draining rivers and coastal waters of Sarawak, Borneo. Biogeosciences, 15, 6847-6865, https://doi.org/10.5194/bg-15-6847-2018, 2018.

Melling, L., Hatano, R., and Goh, K. J. Methane fluxes from three ecosystems in tropical peatland of Sarawak, Malaysia. Soil Biol Biochem 37: 1445-1453, doi:10.1016/j.soilbio.2005.01.001, 2005.

Milliman, J. D., and Farnsworth, K. L.: River Discharge to the Coastal Ocean: A Global Synthesis. Cambridge University Press, March 2011.

Moore, S., Gauci, V., Evans, C. D., and Page, S. E. Fluvial organic carbon losses from a Bornean blackwater river. Biogeosciences 8: 901-909. doi: 10.5194/bg-8-901-2011, 2011.

Moore, S., Evans, C. D., Page, S. E., Garnett, M. H., Jones, T. G., Freeman, C., Hooijer, A., Wiltshire, A. J., Limin, S. H., and Gauci, V. Deep instability of deforested tropical peatlands revealed by fluvial organic carbon fluxes. Nature 493: 660–663. Doi:10.1038/nature11818, 2013.

Müller, D., Warneke, T., Rixen, T., Müller, M., Jamahari, S., Denise, N., Mujahid, A., and Notholt, J. Lateral carbon fluxes and CO_2 outgassing from a tropical peat-draining river. Biogeosciences 12: 5967-5979. doi: 10.5194/bg-12-5967-2015, 2015.

Müller, D., Warneke, T., Rixen, T., Müller, M., Mujahid, A., Bange, H. W., and Notholt, J. Fate of terrestrial organic carbon and associated CO_2 and CO emissions from two Southeast Asian estuaries. Biogeosciences 13: 691-705. doi: 10.5194/bg-13-691-2016, 2016.

Nachtergaele, F., van Velthuizen, H., and Verelst, L.: Harmonized World Soil Database. Path: http://www.fao.org/docrep/018/aq361e/aq361e.pdf. (last access: 29th June 2018), 2009.

Ni, H.-G., Lu, F.-H., Luo, X.-L., Tian, H.-Y. and Zeng, E. Y. Riverine inputs of total organic carbon and suspended particulate matter from the Pearl River Delta to the coastal ocean off South China. Mar Pollut Bull 56: 1150-1157, doi: 10.1016/j.marpolbul.2008.02.030, 2008.

Nightingale, P. D., Malin, G., Law, C. S., Watson, A. J., Liss, P. S., Liddicoat, M. I., Boutin, J., and Upstill-Goddard, R. C. In situ evaluation of air-sea gas exchange parameterizations using novel conservative and volatile tracers. Global Biogeochem Cy 14(1): 373-387, 2000.

Oakes, J. M., Eyre, B. D., Ross, D. J. and Turner, S. D. Stable isotopes trace estuarine transformations of carbon and nitrogen from primary- and secondary-treated paper and pulp mill effluent. Environ Sci Technol 44, 7411-7417, doi: 10.1021/es101789v, 2010.

Oliveira, A. P., Cabecadas, G., and Mateus, M. D. Inorganic carbon distribution and CO_2 fluxes in a large European estuary (Tagus, Portugal). Nature Sci Rep 7: 7376. doi:10.1038/s41598-017-06758-z, 2017.

Page, S. E., Rieley, J. O., and Banks, C. J. Global and regional importance of the tropical peatland carbon pool. Glob Change Biol 17: 798-818. doi: 10.1111/j.1365-2486.2010.02279.x, 2011.

Park, J.-H., Nayna, O. K., Begum, M. S., Chea, E., Hartmann, J., Keil, R. G., Kumar, S., Lu, X., Ran, L., Richey, J. E., Sarma, V.V.S.S., Tareq, S. M., Xuan, D. T., and Yu, R. Reviews and syntheses: Anthropogenic perturbations to carbon fluxes in Asian river systems – concepts, emerging trends, and research challenges. Biogeosciences 15: 3049-3069. doi: 10.5194/bg-15-3049-2018, 2018.

Pataki, D. E., Ehleringer, J. R., Flanagan, L. B., Yakir, D., Bowling, D. R., Still, C. J., Buchmann, N., Kaplan, J. O. And Berry, J. A. The application and interpretation of Keeling plots in terrestrial carbon cycle research, Global Biogeochm. Cycles, 17(1), 1022, doi: 10.1029/2001GB001850, 2003.

Polsenaere, P. and Abril, G. Modelling CO_2 degassing from small acidic rivers using water pCO_2, DIC and δ^{13}C-DIC data. Geochim Cosmochim Acta 91: 220-239, doi: 10.1016/j.gca.2012.05.030, 2012.

Raymond, P. A., and Cole, J. J. Gas exchange in rivers and estuaries: Choosing a gas transfer velocity. Estuaries 24 (2): 312-317, 2001.

Raymond, P. A., Zappa, C. J., Butman, D., Bott, T. L., Potter, J., Mulholland, P., Laursen, A. E., McDowell, W. H., and Newbold, D. Scaling the gas transfer velocity and hydraulic geometry in streams and small rivers. Limnol Oceanogr Fluids and Environments 2: 41-53, doi: 10.1215/21573689-1597669, 2012.

Raymond, P. A., Hartmann, J., Lauerwald, R., Sobek, S., McDonald, C., Hoover, M., Butman, D., Striegl, R., Mayorga, E., Humborg, C., Kortelainen, P., Dürr, H., Meybeck, M., Ciais, P. and Guth, P. Global carbon dioxide emissions from inland waters. Nature, 503:355–359. doi: 10.1038/nature12760, 2013.

Rixen, T., Baum, A., Wit, F., and Samiaji, J. Carbon leaching from tropical peat soils and consequences for carbon balances. Front Earth Sci 4:74. doi: 10.3389/feart.2016.00074, 2016.

Rosentreter, J. A., Maher, D. T., Erler, D. V., Murray, R. And Eyre, B. D. Factors controlling seasonal CO_2 and CH_4 emissions in three tropical mangrove-dominated estuaries in Australia. Under review for Estuar Coast Shelf S, 2018.

Rózanski, K., Froehlich, K., and Mook, W. G. Environmental Isotopes in the Hydrological Cycle. Principles and Applications. Vol. 3: Surface Water. International Atomic Energy Agency and United Nations Educational, Scientific and Cultural Organization, Krakow/Vienna/Groningen, 2003.

Sa'adi, Z., Shahid, S., Ismail, T., Chung, E.-S., and Wang, X.-J. Distributional changes in rainfall and river flow in Sarawak, Malaysia. Asia-Pac. J. Atmos. Sci. 53(4): 489-500. doi: 10.1007/s13143-017-0051-2, 2017.

Sarawak Energy: About Hydropower. Path: http://www.sarawakenergy.com.my/index.php/hydroelectric-projects (last access: 29th June 2018), 2013.

Scofield, V., Melack, J. M., Barbosa, P. M., Amaral, J. H. F., Forsberg, B. R., and Farjalla, V. F. Carbon dioxide outgassing from Amazonian aquatic ecosystems in the Negro River basin. Biogeochemistry 129: 77-91, doi: 10.1007/s10533-016-0220-x, 2016.

Snoussi, M., Haida, S., and Imassi, S., Effects of the construction of dams on the water and sediment fluxes of the Moulouya and the Sebou Rivers, Morocco. Reg Environ Change 3: 5-12. doi: 10.1007/s10113-001-0035-7, 2002.

Staub, J. R. and Esterle, J. S. Provenance and sediment dispersal in the Rajang River delta/ coastal plain system, Sarawak, East Malaysia. Sedimentary Geology 85: 191-201, 1993.

Staub, J. R. and Gastaldo, R. A. Late Quarternary Sedimentation and peat development in the Rajang River Delta, Sarawak, East Malaysia. In: F. Hasan Sidi, Nummedal, D., Imbert, P., Darman, H., and Posamentier, H. W. Tropical Deltas of Southeast Asia – Sedimentology, Stratigraphy, and Petroleum Geology. SEPM Special Publication No. 76, p. 71-87, Tulsa, Oklahoma, USA, September 2003.

Staub, J. R., Among, H. L., and Gastaldo, R. A. Seasonal sediment transport and deposition in the Rajang River delta, Sarawak, East Malaysia. Sediment Geol 133: 249-264, 2000.

Teodoru, C. R., Nyoni, F. C., Borges, A. V., Darchambeau, F., Nyambe, I., and Bouillon, S. Dynamics of greenhouse gases (CO_2, CH_4, N_2O) along the Zambezi River and major tributaries, and their importance in the riverine carbon budget. Biogeosciences 12: 2431-2453. doi: 10.5194/bg-12-2431-2015, 2015.

Thirumalai, K., DiNezio, P. N., Okumura, Y, and Deser, C., Extreme temperatures in Southeast Asia caused by El Nino and worsened by global warming. Nat Commun 8: 15531. doi: 10.1038/ncomms15531, 2017.

Van Asperen, H., Warneke, T., Sabbatini, S., Höpker, M., Nicolini, G., Chiti, T., Papale, D., Böhm, M., and Notholt, J. Diel variation in isotopic composition of soil respiratory CO_2 fluxes: The role of non-steady state conditions. Agricultural and Forest Meteorology 234-235: 95-105, doi: 10.1016/j.agrformet.2016.12.014, 2017.

Venkiteswaran, J. J., Schiff, S. L. And Wallin, M. B. Large carbon dioxide fluxes from headwater boreal and sub-boreal streams. PLOS one, 9(7): e101756, doi:10.1371/journal.pone.0101756, 2014.

Vörösmarty, C. J., Meybeck, M., Fekete, B., Sharma, K., Green, P., and Syvitski, J. P. M. Anthropogenic sediment retention: major global impact from registered river impoundments. Global Planet Change 39: 169-190, 2003.

Wanninkhof, R. Relationship between wind speed and gas exchange over the ocean. J of Geophys Res 97(C5): 7373-7382, 1992

Weiss, R. Carbon dioxide in water and seawater: The solubility of a non-ideal gas. Mar Chem 2: 203—215, 1974.

White, J. W. C., Vaughn, B. H. and Michel S.E., Stable Isotopic Composition of Atmospheric Carbon Dioxide (^{13}C and ^{18}O) from the NOAA ESRL Carbon Cycle Cooperative Global Air Sampling Network, 1990-2014, Version: 2015-10-26, Path: ftp://aftp.cmdl.noaa.gov/data/trace_gases/co2c13/flask/, University of Colorado, Institute of Arctic and Alpine Research (INSTAAR), 2015.

Wit, F. Carbon footprints of peatland degradation. PhD Thesis, University of Bremen, Bremen, Germany, 2017.

Wit, F., Müller, D., Baum, A., Warneke, T., Setiyo Pranowo, W., Müller, M., and Rixen, T. The impact of disturbed peatlands on river outgassing in Southeast Asia. Nat Commun 6: 10155. doi:10.1038/ncomms10155, 2015.

WTW GmbH: FDO 925 and FDO 925-P Operating Manual, Weilheim, Germany, 11/2012.

Yao, G., Gao, Q., Wang, Z., Huang, X., He, T., Zhang, Y., Jiao, S. and Ding, J. Dynamics of CO_2 partial pressure and CO_2 outgassing in the lower reaches of the Xijiang River, a subtropical monsoon river in China. Sci Total Environ 376: 255-266, doi :10.1016/j.scitotenv.2007.01.080, 2007.

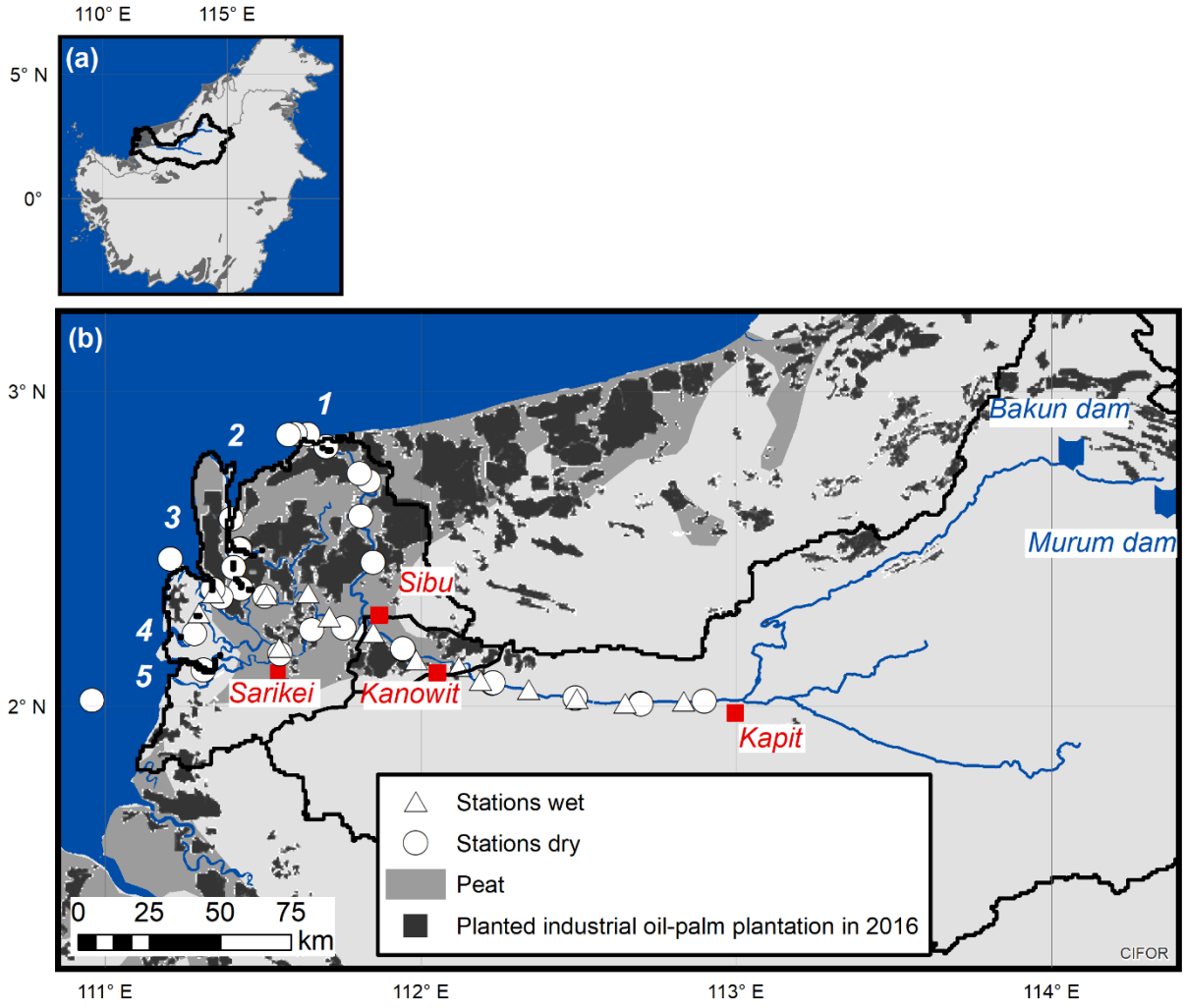

Figure 1: Map of the Rajang basin on the island of Borneo (a) and a close-up of the basin (b) including the location of the peatlands (Nachtergaele et al., 2009), industrial oil palm plantations (Gaveau et al., 2016) and the stations during the cruise. The distributaries are marked with numbers: 1-Igan, 2-Lassa, 3-Paloh, 4-Belawai, 5-Rajang.

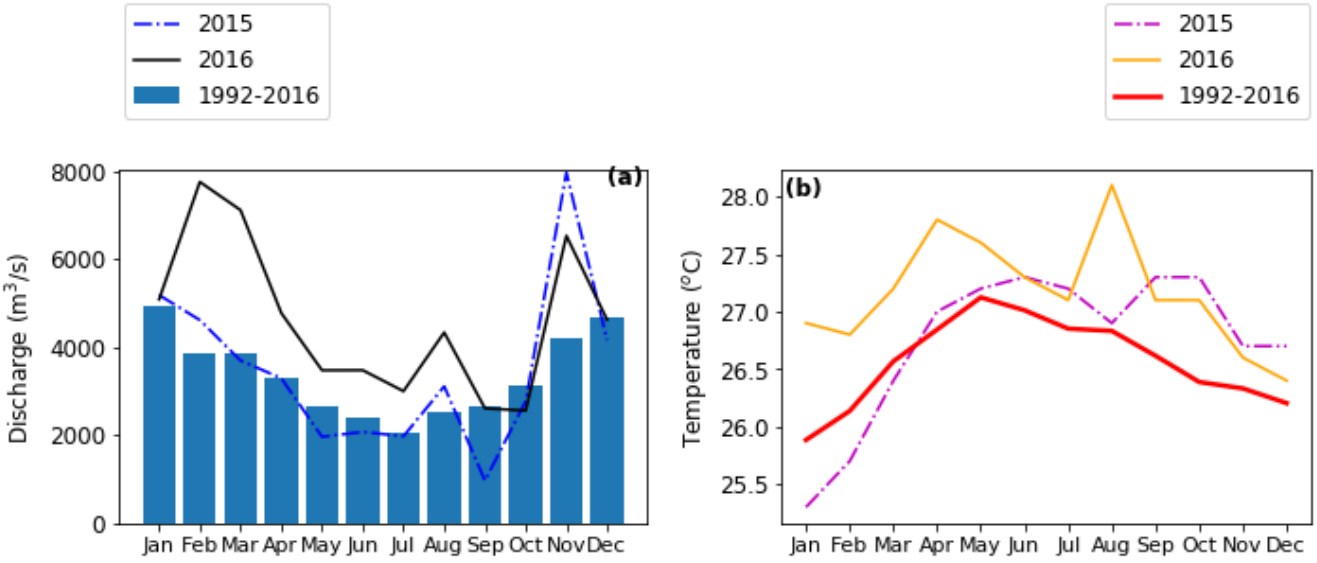

Figure 2: Monthly discharge calculated for the Rajang River (a) and average temperatures (b) for the city of Sibu (2° 20' N, 111° 50' E) for the years 2015, 2016 and the long-term average from 1992-2016. Data from DWD (2018).

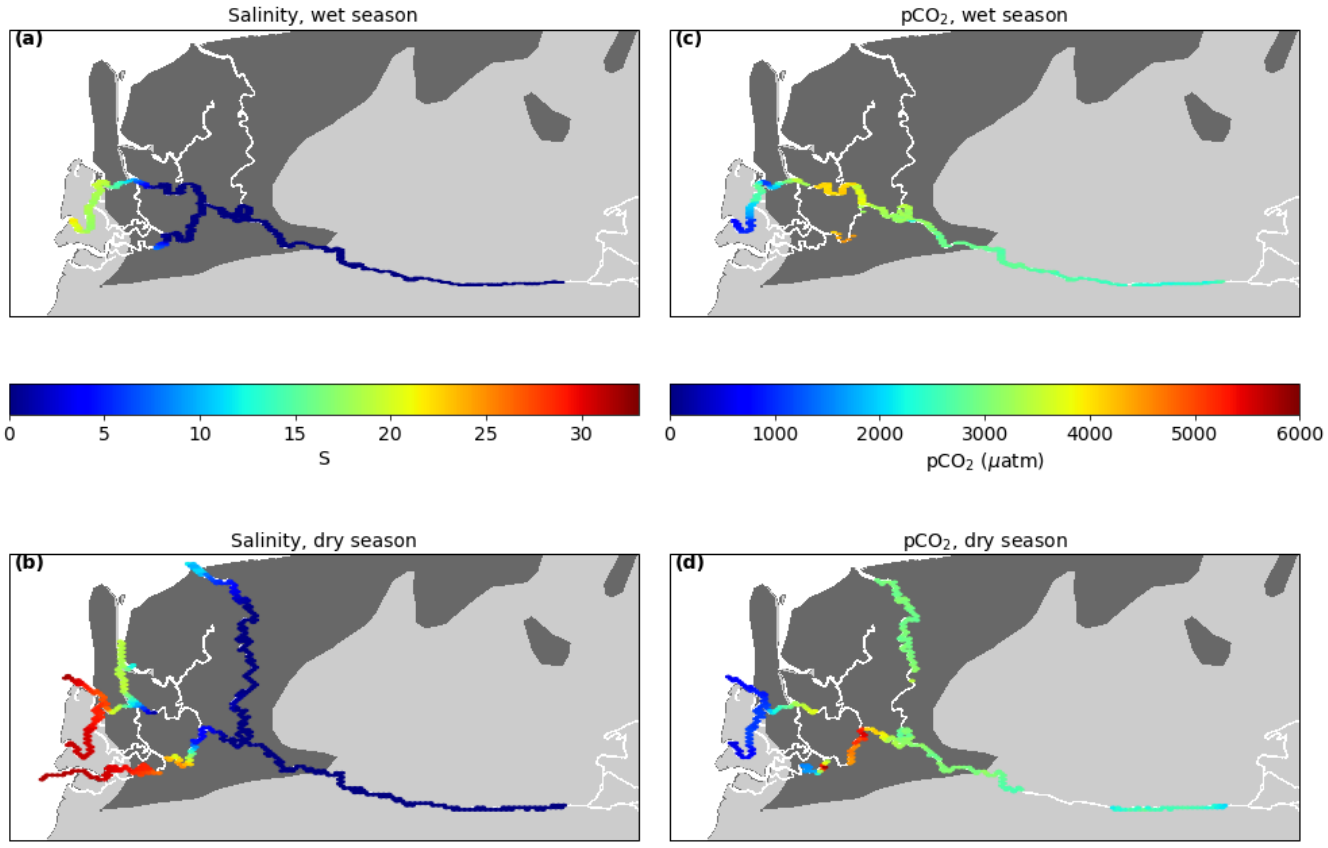

Figure 3: Salinity (interpolated) and *p*CO$_2$ distribution in the Rajang River and delta during the wet season survey (a,c) and dry season survey (b,d).

5

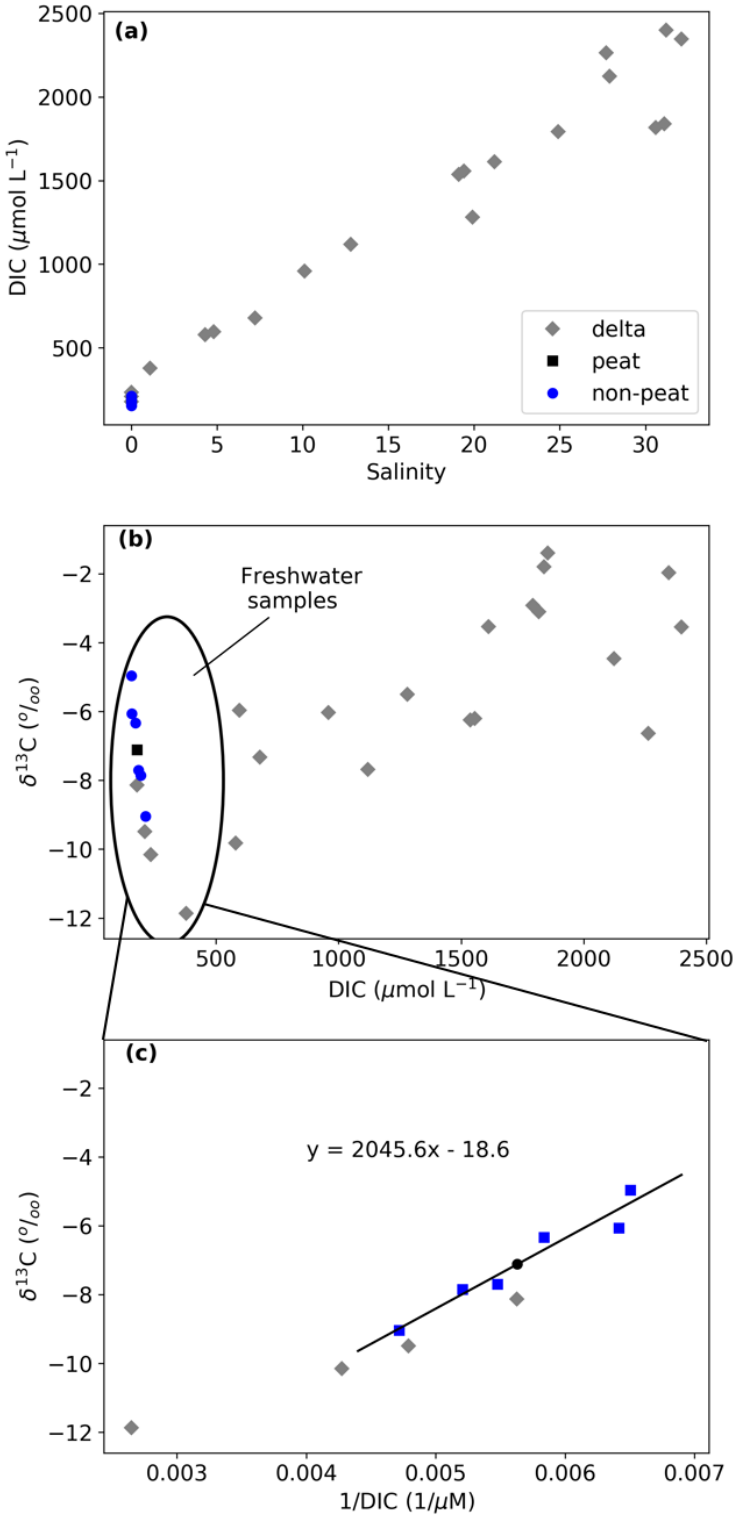
(a)
DIC (μmol L−1)
Salinity
delta
peat
non-peat
(b)
Freshwater samples
δ13C (‰)
DIC (μmol L−1)
(c)
y = 2045.6x - 18.6
δ13C (‰)
1/DIC (1/μM)

Figure 4: DIC versus salinity (a), $\delta^{13}C$ versus DIC (b) and a Keeling plot of $\delta^{13}C$ versus 1/DIC for non-peat, peat and delta samples, respectively. Freshwater samples, including those from the delta region, are circled in in panel b, and only those are shown in the Keeling plot in panel c. All data refer to dry season samples.

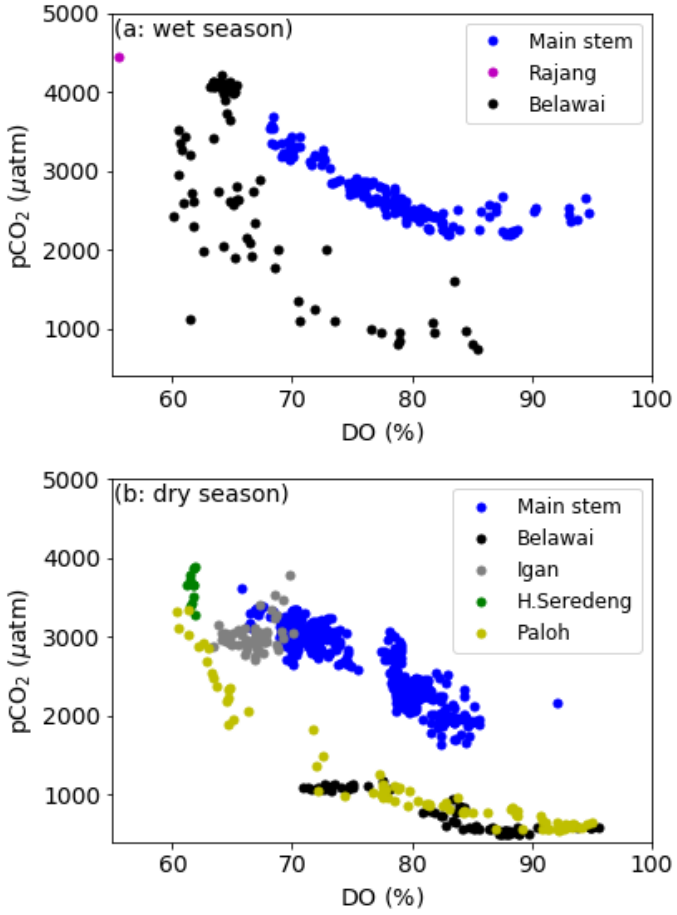

Figure 5: Correlation of pCO_2 versus dissolved oxygen (DO) in the wet and dry season for individual distributaries.

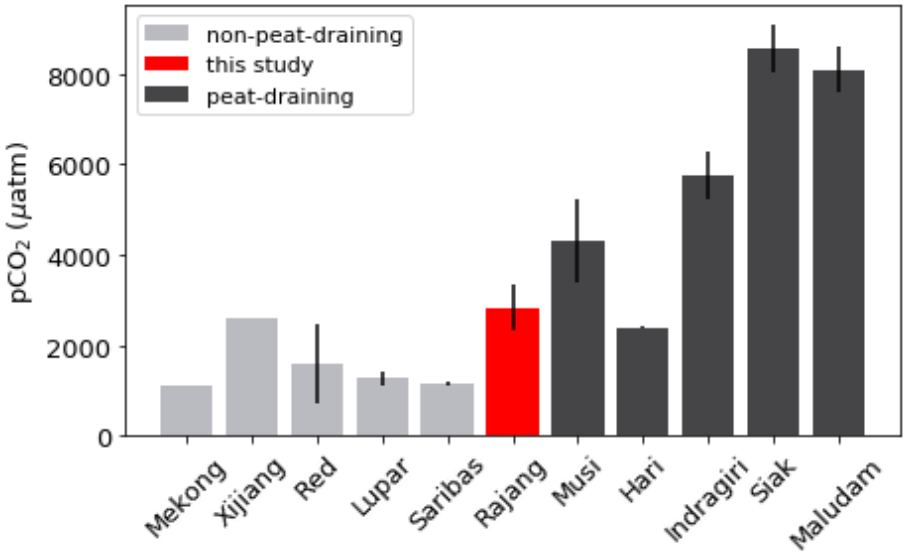

Figure 6: Comparison of average *p*CO_2 values in Southeast Asian rivers. Colors distinguish peat-draining rivers from non-peat-draining rivers. The Rajang River (this study) is highlighted in red.

Table 1: Definition of the different areas considered in this study.

	Non-peat	Peat	Delta
Description of geographical extent	Source to Kanowit	Kanowit to Sibu	Sibu to coast
Definition of geographical extent	lon >112.1000	112.1000 ≥lon ≥111.8193, lat ≤2.2831	lon <111.8193 or lat >2.2831
Water surface area (km²)	167.5	34.3	553.0
Corresponding catchment area (km²)	43550.5	899.6	7559.5
Tidal influence	None	Tidal	Tidal
Influence of salinity	Freshwater	Freshwater	Brackish

Table 2: Average values of measured parameters for different river reaches (mean ± 1SE) for all parameters except FCO2, which is reported as mean (minimum – maximum).

		Non-peat	Peat	Weighted mean peat/non-peat	Delta
Average salinity	**Wet**	0	0	0	7.1± 8.6 (n=566)
	Dry	0	0	0	16.0 ± 13.5 (n=2510)
Temperature (°C)	**Wet**	27.4 ± 0.4 (n=152)	28.7 ± 1.2 (n=89)	27.4 ± 0.4	28.6 ± 1.0 (n=126)
	Dry	28.4 ± 0.6 (n=628)	29.6 ± 0.2 (n=130)	28.4 ± 0.6	30.3 ± 2.6 (n=787)
SPM (mg L^{-1})	**Wet**	188.9 ±76.9 (n=6)	104.5 ± 16.7 (n=2)	187.2 ± 75.7	162.4 ± 88.3 (n=7)
	Dry	51.9 ± 12.3 (n=7)	33.1 ± 2.5 (n=2)	51.5 ± 12.1	68.3 ± 31.6 (n=22)
POC (mg L^{-1})	**Wet**	2.6 ± 0.6 (n=6)	1.8 ± 0.0 (n=2)	2.6 ± 0.6	2.9 ± 2.8 (n=7)
	Dry	1.1 ± 0.4 (n=7)	0.8 ± 0.0 (n=2)	1.1 ± 0.4	1.0 ± 0.4 (n=22)
OC content in SPM	**Wet**	1.5 ± 0.4 (n=6)	1.7 ± 0.3 (n=2)	1.5 ± 0.4	1.6 ± 0.6 (n=7)
(%)	**Dry**	2.1 ± 0.6 (n=7)	2.5 ± 0.0 (n=2)	2.1 ± 0.6	1.5 ± 0.7 (n=22)
O_2 (%)	**Wet**	81.1 ± 5.4 (n=152)	80.8 ± 9.2 (n=89)	81.1 ± 5.5	66.0 ± 6.9 (n=126)
	Dry	79.8 ± 3.5 (n=628)	71.6 ± 1.3 (n=130)	79.6 ± 3.5	71.2 ± 11.1 (n=787)
pH	**Wet**	6.7 ± 0.1 (n=6)	6.6 ± 0.1 (n=2)	6.7 ± 0.1	6.9 ± 0.5 (n=7)
	Dry	6.8 ± 0.0 (n=7)	6.8 ± 0.0 (n=2)	6.8 ± 0.0	7.3 ± 0.5 (n=24)
DIC (µmol L^{-1})	**Wet***	290.8 ± 32.8* (n=5)	243.6* (n=1)	289.8 ± 32.1	338.1 ± 41.9* (n=7)
	Dry	177.9 ± 22.4 (n=6)	177.6 (n=1)	177.9 ± 22.4	1302.3 ± 749.2 (n=21)
δ^{13}C-DIC (‰)	**Dry**	-6.99 ± 1.47 (n=6)	-7.11 (n=1)	-7.0 ± 1.47	-5.90 ± 2.96 (n=21)
***p*CO_2 (uatm)**	**Wet**	2531 ± 188 (n=703)	2990 ± 239 (n=170)	2540 ± 189	3005 ± 1039 (n=566)
	Dry	2337 ± 304 (n=1259)	2994 ± 141 (n=644)	2350 ± 301	2783 ± 1437 (n=2510)
FCO_2	**Wet**	1.5 (0.5-2.0)	1.8 (0.7-2.4)	1.5 (0.5-2.0)	1.8 (0.7-2.4)
(gC m^{-2} d^{-1})	**Dry**	1.7 (0.6-2.6)	2.3 (0.8-3.5)	1.7 (0.6-2.6)	2.0 (0.7-3.0)

Table 3: Average discharge and calculated carbon loads and emissions to the atmosphere, estimated for the months of the two surveys and the whole year 2016.

	Jan 2016	August 2016	Annual estimate 2016
	Peat and non-peat area		
Discharge	4347 $m^3 s^{-1}$	3706 $m^3 s^{-1}$	3942 $m^3 s^{-1}$
DOC load	24 ± 4 GgC/month	21 ± 6 GgC/month	269 ± 60 GgC/year
POC load	30 ± 7 GgC/month	11 ± 4 GgC/month	246 ± 64 GgC/year
DIC load	41 ± 5 GgC/month	21 ± 3 GgC/month	371 ± 46 GgC/year
CO_2 emissions	10 (3-13) GgC/month	11 (4-17) GgC/month	126 (44-181) GgC/year
	Delta		
Discharge ($m^3 s^{-1}$)	739 $m^3 s^{-1}$	630 $m^3 s^{-1}$	670 $m^3 s^{-1}$
CO_2 emissions	31 (12-41) GgC/month	34 (12-51) GgC/month	391 (144-555) GgC/year

Table 4: pCO_2, pH and CO_2 evasion of several Southeast Asian rivers flowing into the South China Sea. *The sampling points were located outside of the peat area, so the actual peat coverage at that point was zero.

	Country	Catchment size (km^2)	Discharge ($m^3\ s^{-1}$)	Peat coverage (%)	pH	pCO_2 (µatm)	CO_2 evasion ($g\ m^{-2}\ d^{-1}$)	Reference
Mekong	Vietnam/Myanmar/Laos/Thailand/Cambodia	795,000	15,000	-	7.4-7.9	1090	2.3	Li et al., 2013
Xijiang	China	350,000	7,290	-	7.6 ± 0.2	2600	2.2-4.2	Yao et al., 2007
Rajang	*Malaysia*	*52,010*	*3,350*	*11*	*6.8 ± 0.1*	*2445 ± 245*	*1.6 (0.5-2.6)*	*This study*
Musi	Indonesia	56,931	3,050	3.5	6.9 ± 0.3	4316 ± 928	7.6 ± 3.2	Wit et al., 2015
Red	China/Vietnam/Laos	156,450	2,640	-	8.1	1589 ± 885	6.4 ± 0.2	Le et al., 2018
Batang Hari	Indonesia	44,890	2,560	5	7.1	2400 ± 18	3.9 ± 0.8	Wit et al., 2015
Indragiri	Indonesia	17,968	1,180	11.9	6.3 ± 0.1	5777 ± 527	10.2 ± 2.7	Wit et al., 2015
Siak	Indonesia	10,423	684	21.9	5.1 ± 0.5	8555 ± 528	14.1 ± 2.7	Wit et al., 2015
Lupar	Malaysia	6,558	490	30.5*	6.9 ± 0.3	1274 ± 148	2.0 ± 0.5	Müller et al., 2016
Saribas	Malaysia	1,943	160	35.5*	7.3	1159 ± 29	1.1 ± 0.9	Müller et al., 2016
Maludam	Malaysia	91	4	100	3.8 ± 0.2	8100 ± 500	9.1 ± 4.7	Müller et al., 2015